Chapter 7

Adaptation to Climate Change at Local Scale: A CFD Study in Porto Urban Area

Vera Rodrigues, Sandra Rafael, Sandra Sorte,
Sílvia Coelho, Hélder Relvas, Bruno Vicente,
Joana Leitão, Myriam Lopes,
Ana Isabel Miranda and Carlos Borrego

Additional information is available at the end of the chapter

http://dx.doi.org/10.5772/intechopen.72972

Abstract

Green infrastructures play an essential role in urban planning, namely with their potential to reduce the impact from air pollution episodes together with extreme weather events. This chapter focuses on the assessment of green infrastructures' benefits on current and future microclimate and air quality patterns in Porto's urban area (Portugal). The effects of green infrastructures on flow dynamics are evaluated for the baseline scenarios by means of numerical and physical simulations, using the computational fluid dynamics (CFD) model VADIS and the wind tunnel of the University of Aveiro. The baseline morphological (BM) scenario focuses on the current morphological characteristics of Porto's urban area, while a baseline green (BG) scenario comprises the replacement of built-up areas by green areas and parks. In addition, the benefits of green infrastructures on air quality are assessed for the baseline and under future climate scenarios. The air quality simulations focus on particulate matter, one of the most critical air pollutants with severe impacts on human health. For the BM scenario, the simulated concentrations are compared with hourly averaged PM10 concentrations measured during a weekday at the air quality station located within the study domain.

Keywords: urban areas, CFD, climate change, adaptation, green infrastructures, future climate scenarios, morphological scenarios

1. Introduction

Despite the advances over the last decades on mitigation of greenhouse gas emissions, climate change still remains a major concern, threatening ecosystems and human systems [1–3]. Currently,

climate change (CC) impacts are recorded worldwide, through extreme weather events, such as heat waves, droughts, floods, cyclones and wildfires [1–3]. In addition, urban areas are facing a continuous unsustainable growth of population [4, 5], associated with extreme weather events and critical air pollution episodes, highly affected by these climate-related events, among other environmental pressures, again threatening human health and lifestyle standards [1–5].

Given the expected increase of extreme weather events, the design and implementation of countermeasures in densely populated urban areas are an important goal in adaptation of societies to climate change in coming decades. Adaptation policies and strategies have the potential to increase resilience of urban areas to climate change, i.e., to improve the ability of a city and the surroundings to readily recover from a disturbance and return to the original functions of the urban metabolism [6]. Recently, several adaptation strategies turn to innovative solutions supported by nature, the so-called nature-based solutions, such as green infrastructures and urban forests, white roofs and highly reflective facades, urban water streams and wetlands, etc. [7–14]. These nature-based solutions provide sustainable, cost-effective, multipurpose and flexible alternatives for tackling societal and environmental challenges, such as climate change, air pollution and human health protection. In particular, green infrastructures (e.g., green roofs, walls and corridors) and urban forests play an essential role in urban planning, leading to several benefits to the environment as solutions of not only resilience to climate change but also to improve air quality and thermal comfort [7–11].

An improved knowledge about the highly complex urban microclimate and consequent air pollutant dispersion patterns is therefore of utmost importance to circumvent climate change impact at local scale (e.g., at street canyon level). A better understanding of the overall urban microclimate, and all the physical- and chemical-related processes, requires not only accurate measurements but also numerical and physical modeling of the exchanges within the urban atmospheric boundary layer [15, 16]. In recent years, several studies have been performed using physical models, such as wind tunnel simulations, experimental campaigns and numerical models [17–29]. In particular, computational fluid dynamics (CFD) models have been used to compute turbulent flow dynamics and atmospheric pollutant dispersion within the urban surface layer. These models usually allow taking into account the morphological specificities of the urban environment, and consequently, they are able to simulate the flow dynamics perturbations caused by distinct urban obstacles [23–29]. Specifically, CFD models have been applied to assess the role of urban vegetation in mitigating air pollution, mainly considering the effects of trees induced by mechanical drag of trees and/or including the pollutant removal capacity of trees by deposition and filtration mechanisms [30–38]. Still, most of the numerical, physical and experimental studies have been performed over urban-like geometries, through idealized configurations and hypothetical scenarios [33]. Although the effects of green infrastructures on urban atmospheric dynamics have been widely studied, a deeper knowledge is still required regarding the overall perturbations induced by trees on turbulent flow dynamics and, consequently, air pollutant dispersion. Up to now, despite the several contributions from outdoor measurements, wind tunnel measurements, extensive database on idealized street canyons and several CFD studies, the current understanding of turbulent flow dynamics within and around vegetation is not sufficient, denoting local increases and decreases of wind speed and turbulence, depending on several parameters (e.g., characteristics of vegetation, urban morphology and meteorological conditions). Therefore, the

first identified knowledge gap, which motivates this work, refers to the need to contribute to improve the knowledge of the effects of green infrastructures on turbulent flow dynamics at a local scale and, consequently, on air pollutant dispersion patterns.

Furthermore, in literature, the study of climate change impacts ranges from global scale down to the regional and urban scale [39, 40] (e.g., in [40] the authors have performed a 10-year air quality projection under climate and city-level emission changes at urban scale applying a horizontal resolution of 4 km × 4 km). Nevertheless, the full understanding of the impact on air quality at a local scale is a challenge and the effects are still unknown. Another identified knowledge gap is the lack of studies focused on local-scale effects, with an insufficient understanding and accurate predictions of the changes in urban microclimate patterns and in pollutant concentrations under climate changes. Air pollutant dispersion is mainly driven by meteorological forces, and thus it is natural that changes in future climate will strongly affect air quality patterns, resulting, potentially, in an increase of the magnitude and frequency of air pollution episodes. Therefore, several issues arise concerning how the changes on global and regional circulations will affect local-scale urban microclimate, how to use GI as an adaptation measure to increase resilience to CC at local scale, and what is the link between the impact of GI under future, past and current climate.

This chapter aims to foster urban microclimate knowledge and to assess CC effects at a local scale, evaluating strategies of adaptation to CC toward an urban sustainable development. The chapter's main objective is to evaluate the impact of distinct resilience measures on the urban microclimate and air quality, in recent past, current and future climate scenarios for Porto's urban area. These resilience measures will be based on green infrastructures.

2. Numerical modeling approach

A cascade of numerical models is applied in this work, from global scale down to local scale (e.g., street canyon and surroundings) to assess the urban microclimate and air quality patterns.

2.1. From global to urban scale

A cascade of numerical models, from global to urban scale, was applied to the Greater Porto area. The numerical model *Weather Research and Forecasting* (WRF) *Model* version 3.7.1 [41] was applied to perform regional climate simulations for Porto city and surrounding areas through dynamical downscaling. WRF setup has included four domains on line nested with increasing resolution at a downscaling ratio of three: domain 1 at 27 km resolution covering West Europe, Atlantic Ocean and North Africa; domain 2 at 9 km resolution over the Iberian Peninsula; domain 3 at 3 km resolution over Portugal; and domain 4 with 1 km resolution over North West Portugal. All these domains were used to perform a representative simulation of the recent past climate (1976–2005) that was used as the reference simulation and a representative simulation of the future medium-term climate (2041–2070). For the future simulation, the Representative Concentration Pathway Scenario RCP8.5 has been adopted, from the new generation of climate change future scenarios included in the Fifth Assessment Report of the Intergovernmental Panel on Climate Change [42]. The MPI-ESM-LR model was used to

provide initial and boundary conditions to WRF model, with a spatial resolution of 1.9° and 47 hybrid sigma-pressure levels (Max Planck Institute for Meteorology Earth System Model) [43].

2.2. CFD numerical formulation

Pollutant DISpersion in the atmosphere under VAriable wind conditions (VADIS) is the CFD model applied to Porto urban area to assess local-scale flow dynamics and air quality. This CFD model was developed by the University of Aveiro to numerically simulate air pollutant dispersion in complex urban areas and under unfavorable wind conditions. VADIS consists of two distinct modules: the FLOW and DISPER.

2.2.1. Turbulent flow dynamics

FLOW is a Eulerian module able to simulate the turbulent flow dynamics under stationary conditions within the atmospheric boundary layer. This module numerically solves by means of finite differences (SIMPLE solver), over a Cartesian tridimensional grid, the Navier-Stokes (NS) equations for the wind velocity components, the turbulent viscosity, pressure and the turbulent kinetic energy, applying Reynolds averages (the so-called Reynolds-Averaged Navier-Stokes [RANS] approach). The equation of mass conservation is written as Eq. (1), while the NS equations for the momentum conservation are given by Eq. (2).

$$\frac{\partial u_i}{\partial x_i} = 0 \tag{1}$$

$$u_j \frac{\partial u_i}{\partial x_i} = -\frac{1}{\rho}\frac{\partial P}{\partial x_i} + \frac{\partial}{\partial x_j}\left(\nu_e \frac{\partial u_i}{\partial x_j}\right) + S_u \tag{2}$$

where ui represents each velocity component (u, v and w) and x_i the spatial coordinates (x, y and z), P denotes the pressure, ρ is the air density, ν_e is the effective viscosity and S_u indicates the source and/or sink term for u_i.

The computation of the NS equations is based on the mechanics of fluid fundamental laws, simplified through a set of considerations and completed with closure formulations, namely in the turbulence simulation. The equation system closure is made through the turbulent isotropic viscosity approach, calculated from the kinetic turbulent energy transport equations and their dissipation rate. The first-order k-ε closure scheme [44] is used to model the turbulent viscosity (ν_t), solving two additional equations for the turbulent kinetic energy (k), Eq. (3), and the dissipation rate (ε), Eq. (4).

$$u_j \frac{\partial k}{\partial x_j} = \frac{\partial}{\partial x_i}\left(\frac{\nu_t}{\sigma_k}\frac{\partial k}{\partial x_i}\right) + \nu_t\left(\frac{\partial u_i}{\partial x_j} + \frac{\partial u_j}{\partial x_i}\right)\frac{\partial u_i}{\partial x_j} - \varepsilon + S_k \tag{3}$$

$$u_j \frac{\partial \varepsilon}{\partial x_j} = \frac{\partial}{\partial x_i}\left(\frac{\nu_t}{\sigma_\varepsilon}\frac{\partial \varepsilon}{\partial x_i}\right) + c_{\varepsilon 1}\frac{\varepsilon}{k}\nu_t\left(\frac{\partial u_i}{\partial x_j} + \frac{\partial u_j}{\partial x_i}\right)\frac{\partial u_i}{\partial x_j} - c_{\varepsilon 2}\frac{\varepsilon^2}{k} + S_\varepsilon \tag{4}$$

where σ_k, σ_ε, $c_{\varepsilon 1}$ and $c_{\varepsilon 2}$ are closure constants set to the standard values of 1, 1.3, 1.44 and 1.92, respectively. S_k and S_ε are the additional source terms of k and ε.

VADIS model is suited for the simulation of the wind field and the turbulent viscosity affected by a set of obstacles (e.g., buildings) localized over the Cartesian grid. The CFD model VADIS

was updated by [31] to consider the aerodynamic effect of urban vegetation, adding source terms to momentum (Eq. (5)), turbulent kinetic energy (Eq. (6)) and its dissipation rate (Eq. (7)) equations, calculated based on tree-airflow interactions, neglecting viscous drag relative to form (or pressure) drag [45, 46].

$$S_u = -C_d LAD|U|\,u_i \tag{5}$$

where C_d is the mechanical drag coefficient, LAD denotes the leaf area density and $|U|$ is the magnitude of the wind speed vector.

S_k denotes the production of turbulence by the action of vegetation elements.

$$S_k = -C_d LAD\left(\beta_p |U|^3 - \beta_d |U| k\right) \tag{6}$$

where β_p is set to 1 and indicates the fraction of the mean flow kinetic energy converted to wake-generated turbulent energy by canopy drag. β_d is set to 4 and denotes the fraction of turbulent energy dissipated by "short-circuiting" of the Kolmogorov cascade [47, 48] and $\beta_d |U| k$ points out the dissipation of the generated wakes [49]. Then, S_k represents the sum of the source and sink of turbulent kinetic energy due to the effect of vegetation elements.

The numerical formulation of S_ε is similar to the formulation of S_k.

$$S_\varepsilon = -C_d LAD\left(c_{\varepsilon 4}\beta_p |U|^3 \frac{\varepsilon}{k} - c_{\varepsilon 5}\beta_d |U| \varepsilon\right) \tag{7}$$

where $c_{\varepsilon 4}$ and $c_{\varepsilon 5}$ are both equal to 1.5.

Therefore, VADIS model is suited for the calculation of the perturbations induced by vegetation elements on the flow dynamics and dispersion patterns.

2.2.2. Pollutant dispersion over complex geometries

The DISPER module uses the data provided by the previously mentioned module, namely the wind field, and estimates the tridimensional concentration field of the air pollutant dispersion, based on the Lagrangian Stochastic approach. This methodology assumes that the pollutant spatial and temporal dispersion is conveniently represented by a large number of numerical particles randomly released in the flow. Langevin equation (Eq. (9)) computes particle displacement at each time step by the sum of the deterministic component obtained from the wind velocity (u_i), the aleatory component (u_i') related with the local turbulence and the influence of the fluctuation forces. T_L is the Lagrangian timescale.

$$d\,u_i = -\left(\frac{u_i}{T_L}\right)dt + du'_i \tag{8}$$

The fundamental Lagrangian equation assumes that each particle is represented by a constant mass quantity. The mean concentration of the pollutant at point X and time t due to the contribution of point X_0 is represented by the probability of occurrence (the probability $P(X_0,X,t)$ of a particle emitted at X_0 to be at point X and at time t) and the concentration at the original point. Then, the sum of the contributions of all points within the computational domain represents the mean concentration at point X and instant t. $C(s)$ is written as [50]:

$$C(X) = \int P(X_0, X, t)\, C_0(X_0) dX_0 \tag{9}$$

The performance of VADIS model has been evaluated by comparison with wind tunnel data, other CFD models and in-situ measurements [31, 50–52].

3. Modeling system application

3.1. Case study

Porto urban area is located in coastal northern Portugal bounded by the Atlantic Ocean and the Douro River. Porto is the second largest city in Portugal with a population of 237,591 inhabitants and the city center of Porto metropolitan area covering 1900 km^2 with more than 1.5 million inhabitants [53]. Porto metropolitan area is characterized by a fast urban expansion with dense residential and commercial areas and a few and sparse green areas. Porto city features a temperate Atlantic climate with warm and dry summers and mild rainy winters [54]. The urban area is surrounded by two metropolitan rings, each one with important links to Porto metropolitan area, in terms of mobility, with high rates of emissions from road traffic. Porto urban area has been selected as the case study in the framework of CLICURB project—"Urban atmospheric quality, climate change and resilience." The main objective of CLICURB project was to improve the scientific knowledge about urban microclimate and to bridge the gap between global climate change trends and urban development considering the inclusion of adaptation strategies on urban planning and decision-making processes. This research project is aimed to identify a set of measures suited for the increase of urban resilience, including the quantification of their effectiveness to mitigate climate change impact. CLICURB project intended to assess the impact of future climate on urban areas at different levels, e.g., meteorology, energy fluxes and air quality. The most relevant outcome of CLICURB was the production of an urban atlas, both for present and mid-twenty-first century, consisting of a series of layers for urban climate, thermal comfort, air pollutant emissions and air quality.

3.1.1. Computational domain

The modeling system was applied following three distinct steps, in order to assess the impact of green infrastructures on flow dynamics and air quality levels, evaluating their effectiveness as green urban planning strategies, under recent past, current and future medium-term climate. The **first step** focuses on the comparison of flow dynamics between wind tunnel and CFD simulation results, for both a baseline and a green scenario. The **second step** includes the comparison of CFD simulation results with PM10 concentrations measured at the air quality station located within the computational domain, for 24th September 2010 (this specific day was selected due to the data availability of traffic counting and meteorological data). The **third step** comprises the simulation of meteorological fields, from global down to urban scale (following the procedure described in section 2.1), as well as the CFD simulation at local scale of the urban microclimate and air quality under recent past climate and future medium-term climate. **Figure 1** shows the selected study area within Porto city center. D1 points out the selected study area for **step 1**, while D2 denotes the selected study area used in **step 2** and **step 3**.

http://dx.doi.org/10.5772/intechopen.72972

Figure 1. Selected study area in Porto city center, with the location of domains D1 and D2.

Figure 2 shows the simulation domain used in the wind tunnel and in the CFD simulations (**step 1**). The study area is centered in part of *Rua da Constituição*, a street canyon located in the city center of Porto. The baseline domain (**Figure 2a**) corresponds to the current morphological conditions of the study area, while the hypothetical green scenario (**Figure 2b**) corresponds to the replacement of two blocks of buildings for parks flanked by groups of trees.

A set of physical simulations were carried out using the wind tunnel facilities of the University of Aveiro, for the baseline and the corresponding green scenario (**Figure 2**), to assess the impact

Figure 2. Computational domain for (a) the baseline scenario and (b) the green scenario, including the wind speed measurement point location, or the corresponding computational cells in the CFD simulations. The newly implemented green areas are represented by green circles.

on local wind of replacing a built-up area by green parks. The wind tunnel experiments were performed using a scaled mock-up within the test section of the tunnel with 6.5 m × 1.5 m × 1 m. For that purpose, a 1:250 scaled interchangeable model of the urban domain D1, covering a full extension of approximately 360 m, was built for both the baseline and the green scenarios corresponding to the domain in **Figure 2a** and **b**. The atmospheric boundary layer was simulated using a specific setup of turbulence generators and floor roughness elements, located upstream the test section. The flow analysis was performed by measurements of the wind speed and turbulence, with a time resolution sampling rate of 0.5 s, using a hot-wire anemometer (TSI IFA-300).

Both the mock-up of the baseline and the green scenario were tested in the wind tunnel. The wind speed was measured at different locations, from points 1 to 8 indicated in **Figure 2b**), at a height corresponding to 1.5 m in full scale. A corresponding set of CFD simulations were performed using VADIS model. The simulated values are extracted at the cell corresponding to the location of the measurement points.

The typical meteorological conditions were established from the analysis of an historical database of climatological data for the northern Portuguese region. The prevailing conditions correspond to a wind blowing from North, West and Southeast. The wind speeds of 3 and 6 m s^{-1}, at 10 m high, were selected as prevailing conditions, while a wind speed of 9 m s^{-1} was selected as representative of strong wind speed conditions.

In **step 2**, the CFD model is applied to an area defined in the city center of Porto (computational domain of 1300 m × 1300 m × 150 m shown in **Figure 3**), which includes the air quality station Francisco Sá Carneiro-Campanhã, mainly influenced by road-traffic emissions. The CFD simulations were performed with a grid resolution of 3 m × 3 m × 3 m in a total of 9,417,800 number of cells. The baseline computational domain is presented in **Figure 3a**, including the

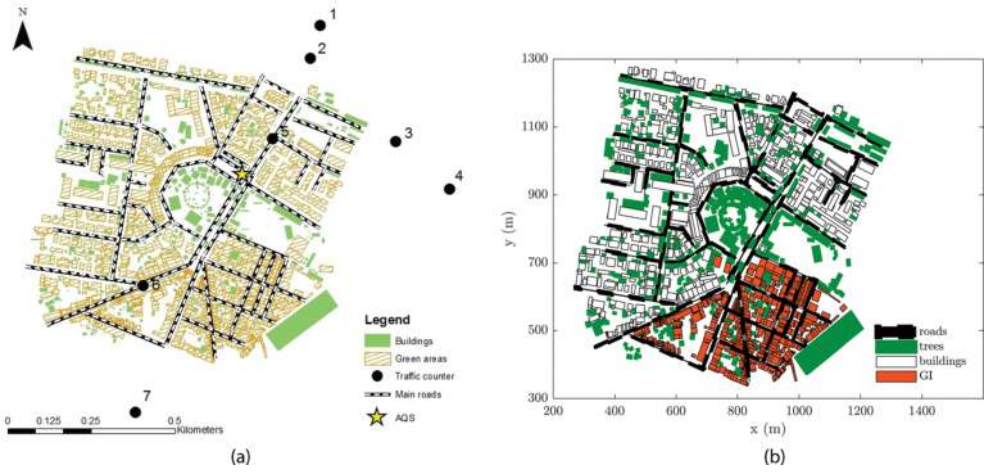

Figure 3. Computational domain for (a) the baseline scenario, including the location of the traffic counter devices, as well as the air quality station; and (b) the green scenario, where the newly implemented green areas are represented by red rectangles (GI).

location of the traffic count devices (1–4 and 7), the air quality station, as well as the location of buildings, trees and roads, corresponding to the current morphological data of the study area. The green scenario is shown in **Figure 3b** and comprises the implementation of green areas in 35% of the current built-up area located in the Southeast part of the domain (pointed out by the red rectangles). Within the newly implemented green areas, the height of trees varies between 3 and 30 m. The overall roads keep the same hourly emission rate as for the baseline scenario.

In the **third step,** the CFD model is also applied to the area defined in the city center of Porto included in the computational domain D2.

3.2. Emissions from road traffic

The traffic roads are defined within the computational domain as line sources (see **Figures 3** and **4**). All these roads were considered as emission sources with an associated emission rate. Hourly averaged PM10 emission rates from on-road transport vehicles were calculated with high temporal and spatial resolution using the *Transport Emission Model for Line Sources (TREM)*. This model was developed at the University of Aveiro, based on MEET/COST319 methodology [50]. The hourly emission rates are estimated for each road segment, considering the local information on traffic counting data. Vehicle counting data was acquired using automatic devices installed in seven distinct locations (**Figure 3a**). Empirical rates expressing the relation with the traffic in the surrounding roads were applied in case of roads without available data.

In addition, the calculation of the emission rates are also based on emission factors following the European guidelines [55] and considering the fleet composition and the characteristics of the vehicles, such as age of vehicles, average speed, engine type, capacity and technology, vehicle weight and fuel consumption (e.g., diesel, gasoline or LPG). TREM algorithm applies an aggregation of vehicles by categories (e.g., passengers, light-duty vehicles, heavy-duty vehicles, busses, motorcycles and new-technology vehicles, such as hybrid and electric cars). For all vehicle categories, 350 classes were considered including EURO1 to EURO5 vehicles and depending on the characteristics of vehicles and their emission standards. Fleet data of the percentage of vehicles in each class were obtained from national databases [56, 57].

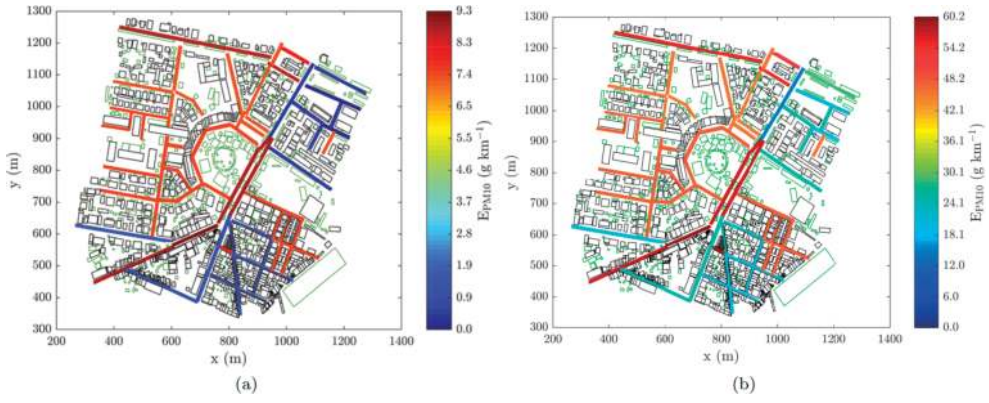

Figure 4. Hourly averaged PM10 emission rates calculated for each road segment at (a) 4 am and (b) 8 am.

Figure 4 shows the hourly averaged PM10 emission rates calculated for each road segment, in 68 segments. The figure points out the variation of PM10 emission rates depending on the road segment for two distinct hours characterized by low emission rates, at 4 am (**Figure 4a**), and high emission rates, at 8 am (**Figure 4b**). The results correspond to a weekday (Friday, 24th September 2010) typical behavior of downtown traffic flow.

The main road in the domain is *Avenida de Fernão Magalhães*, constituted by five lanes, i.e., three on the right side and two on the left, from South to North direction, separated by a central row of trees. This main avenue is divided into four road segments, for the computation of the emission rates. The two parallel road segments with high emission rates are located in the intersections with the roundabout where the Air Quality Station is located. On the contrary, the low emission rates are registered in the road segments located in the Southeast neighborhood of the computational domain.

Figure 5 presents the calculated PM10 emission rates in an hourly basis: the minimum, the maximum and the average values. The minimum values are recorded in several road segments in the Southeast part of the domain, while the maximum values are always registered in the main avenue. The average curve corresponds to the average of the hourly emission rates estimated for all the 68 road segments.

The maximum emission rates registered at 4 and 8 am are equal to 9.2 and 60.2 g km^{-1} h^{-1}, respectively, while the minimum rates are equal to 0.12 g km^{-1} h^{-1} at 4 am and to 14.9 g km^{-1} h^{-1} at 8 am. The high emission levels are registered during the morning, after 8 am, until evening, while the low emission levels are estimated during the night.

3.3. Meteorological inflow boundary conditions

Several CFD simulations were performed over the computational domain D2, in the **second step**, for 24th September 2010, for both the baseline morphological and the baseline green scenarios. The meteorological inflow conditions for these CFD simulations were obtained from mesoscale simulations using WRF model [41]. The mesoscale simulations were conducted over Continental Portugal with a horizontal grid resolution of 5 km. The meteorological data for 24th September 2010 are presented in **Figure 6**, i.e., the hourly average wind speed (**Figure 6a**) and wind direction (**Figure 6b**).

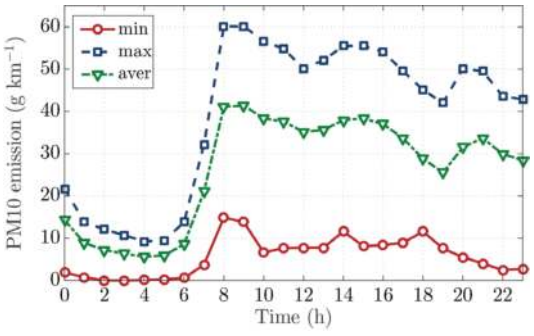

Figure 5. Hourly maximum, minimum and average values of PM10 emissions.

http://dx.doi.org/10.5772/intechopen.72972

The hourly wind speed (**Figure 6a**) ranges from low to moderate wind speed conditions, between 0.1 m s^{-1}, during the night at 5 am, and 6.5 m s^{-1}, during the afternoon at 3 pm, while the wind direction (**Figure 6b**) varies from South-Southwest to North-Northeast, blowing predominantly from the 4th quadrant. The high wind speed is registered during daylight time, between 8 am and 6 pm. In addition, the friction velocity ranges from a minimum near zero to a maximum of 1 m s^{-1}. The aerodynamic roughness length was calculated in an hourly basis from the vertical wind profile and ranges from 0.8 to 2.2 m.

3.4. Meteorological data for recent past and future medium-term climate

The meteorological results in **Figure 7** show the greatest reduction of wind speed in the first autumn months in the mid-term future climate, compared to the recent past climate. For the remaining seasons, the simulation results only show negligible variations with any clear trend. The simulation results show a slight decrease in the average number of days with moderate to strong wind speed or higher and a slight increase in the average number of days recording low wind speed conditions, in the future medium-term climate.

Temperature data show an annual average increase of about 1.1°C in the mid-term future climate. **Figure 8** shows the minimum and maximum monthly values of temperature, together with the monthly average values. Monthly maximum temperatures increase almost every month. The highest anomaly records are projected for summer and autumn, e.g., in July (one of the hottest months), the anomaly points out an increase of 5°C. The monthly minimum temperatures also increase, again with the largest anomalies occurring in the summer and autumn time.

The number of heat waves in the mid-term future climate increases about seven times compared to recent past climate. The average of duration of the heat waves also increases and the days with the maximum temperature greater than 35°C increase 4 times. The results also show an increase in the number of summer days and tropical nights. Although for the recent past climate the greatest number of heat waves occurs during spring and summer time, in the mid-term future climate, these extreme events will occur in summer and autumn time.

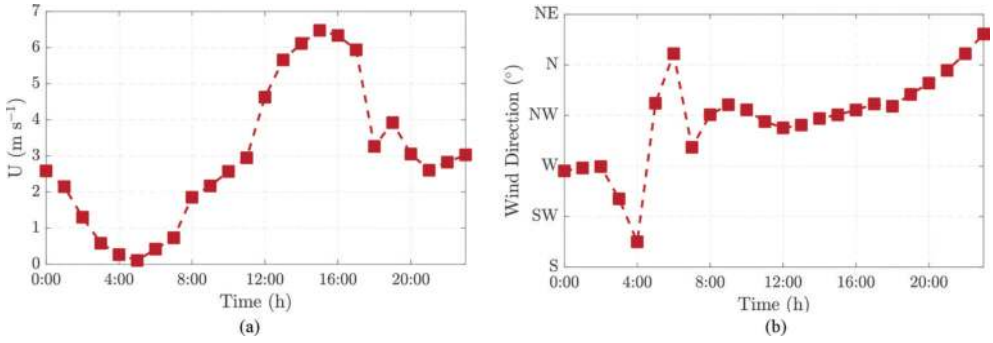

Figure 6. Hourly meteorological data, for 24th September 2010, simulated using the WRF model and used as inflow data in the CFD simulations: (a) wind speed and (b) wind direction.

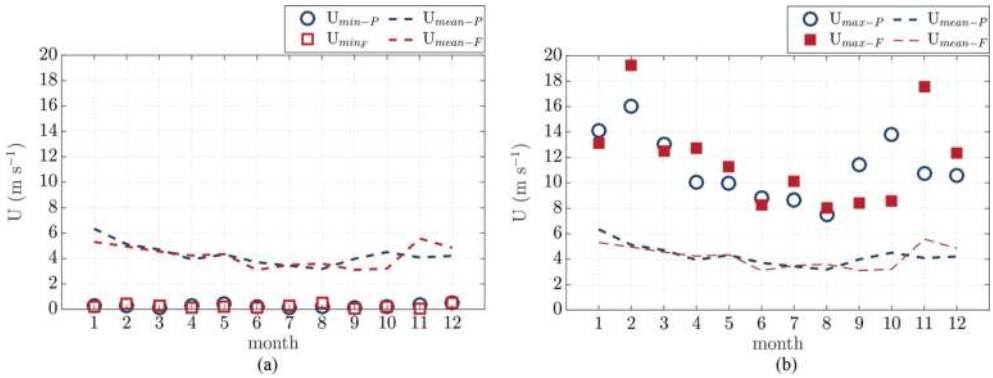

Figure 7. Extreme events recorded in the recent past and the future medium-term climate: (a) minimum and (b) maximum monthly values of wind speed, together with the monthly average values.

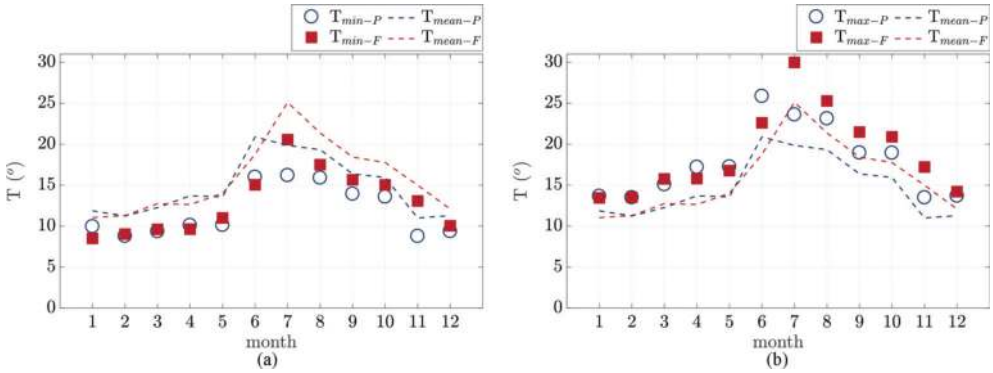

Figure 8. Extreme events recorded in the recent past and the future medium-term climate: (a) minimum and (b) maximum monthly values of temperature, together with the monthly averaged values.

4. Assessment of GI effects on flow dynamics using CFD and wind tunnel simulations

The effects of green infrastructures on flow dynamics are assessed by comparison between the baseline morphological scenario and the corresponding green scenario, in the first step of this study. Then, the accuracy of the numerical and physical results is evaluated through the comparison between both results and the estimation of statistical parameters.

4.1. Impact of GI on flow dynamics

Figure 9 shows the measured and simulated data for the baseline and the green scenarios and for an inflow wind blowing from North with wind speeds of 3 and 9 m s^{-1}, as example.

http://dx.doi.org/10.5772/intechopen.72972

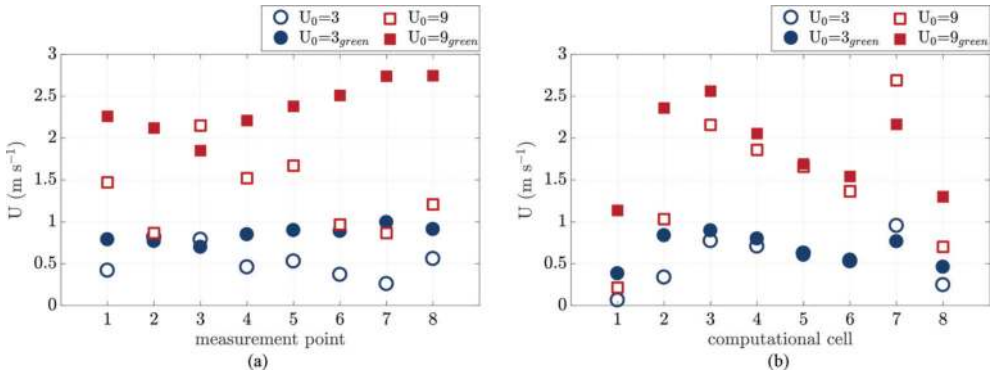

Figure 9. Comparison between the wind speed from the baseline and the green scenario: (a) measured in the wind tunnel and (b) simulated with the CFD model. These results are obtained from the numerical and physical simulations with an inflow wind blowing from North.

Hereafter, the effects of GI are studied in terms of increase or decrease of wind speed registered in the green scenario, when compared to the baseline. In the specific case of an inflow wind from North direction, point 8 is located immediately upstream from a barrier of trees, within one of the implemented green parks. At this location, both the CFD and wind tunnel results are in accordance, predicting an increase of wind speed in the green scenario. The increase of wind speed ranges between 0.4 and 1.5 m s^{-1} in the wind tunnel measurements, and between 0.3 and 0.9 m s^{-1}, in the CFD simulations, corresponding to an inflow wind speed of 3 and 9 m s^{-1}, respectively. Following in this section, the data analysis consistently correspond to an inflow wind speed of 3 and 9 m s^{-1}, respectively. Points 1 and 6 are located in the West and East boundaries of the street canyon, and in those points, both CFD and wind tunnel results point out an increase of wind speed. CFD results indicate an increase of wind speed, within the cell corresponding to the point 1 location, of 0.5 and 1.4 m s^{-1}, while the wind tunnel measurements denote an increase of 0.4 and 0.8 m s^{-1}. In point 6, the CFD model simulates a negligible increase of wind speed of 0.02 m s^{-1} and then an increase of 0.3 m s^{-1} (in the simulation with an inflow wind speed of 9 m s^{-1}). The wind tunnel results show an increase of wind speed of 0.5 and 1.5 m s^{-1}. Immediately downstream the newly implemented green parks are located points 2 and 7. CFD results show an increase of 0.4 and 1.4 m s^{-1}, in point 2, and a decrease of 0.3 and 0.5 m s^{-1} in point 7, whereas the wind tunnel measurements point out a negligible decrease of 0.1 m s^{-1} and an increase of 1.3 m s^{-1}, for inflow wind speeds of 3 and 9 m s^{-1}, in point 2, and an increase of 0.7 and 1.9 m s^{-1}, in point 7. Points 3–5 are located downstream far from the main avenue, but the results indicate some perturbations exerted by GI. CFD results show an increase of 0.2 and 0.6 m s^{-1}, in point 3, an increase of 0.1 and 0.3 m s^{-1}, in point 4, and a slight decrease of 0.03 m s^{-1} and a slight increase of 0.1 m s^{-1}, in point 5. The wind tunnel data show a decrease of 0.1 and 0.3 m s^{-1}, in point 3, and an increase of 0.4 and 0.7 m s^{-1}, for both points 4 and 5.

In conclusion, both numerical and physical results point out an overall increase of wind speed and a good agreement between CFD simulations and wind tunnel measurements to predict this trend. Exceptions are found in point 3, in the wind tunnel results, and in point 7, in CFD simulations, where a decrease of wind speed is registered.

Figure 10 presents the measured and simulated data for an inflow wind blowing from West. The effects of GI are over again studied in terms of increase or decrease of wind speed registered in the green scenario, when compared to the baseline.

In the specific case of an inflow wind from West direction, point 1 is located at the inlet of the domain and upstream the newly implemented green areas. At this location, the wind tunnel results present negligible differences of wind speed for the green scenario compared to the baseline. However, at the same location, the CFD results show a more significant impact of the green scenario pointing out a decrease of 0.4 and 1.4 m s^{-1}, in the simulations with inflow wind speeds of 3 and 9 m s^{-1}. Points 2 and 7 are located in the main avenue of the street canyon, near the adapted area, and are strongly affected by the presence of the new green areas. The wind tunnel results show an increase of 0.2 and 0.5 m s^{-1}, in point 2, and an increase of 0.5 and 1.5 m s^{-1}, in point 7. Thus, the location downstream in the street canyon is more affected by the GI. On the contrary, in CFD simulations, the effects of GI are more relevant in point 2, with an increase of wind speed of 1 and 3 m s^{-1}, while in point 7, an increase of 0.1 and 0.4 m s^{-1} is registered. Therefore, CFD and wind tunnel results are not in good agreement if analyzed in-depth locally. At the location of point 8 within the second green park, the wind tunnel results show an increase of 0.5 and 1.3 m s^{-1}, while the CFD results show a slight decrease of 0.3 and 0.6 m s^{-1}. Points 3 and 4 are located away from the intervention area, and an insignificant effect was theoretically expected. However, the wind tunnel results show an increase of wind speed of 0.8 and 2.1 m s^{-1}, in point 3, and an increase of 0.5 and 1.4 m s^{-1}, in point 4. CFD results point out an increase of wind speed of 0.5 and 1.4 m s^{-1}, in point 3, and a decrease of wind speed of 1 and 2.1 m s^{-1}, in point 4. At the locations of points 5 and 6, at the outlet of the domain, CFD results show negligible increases of wind speed, less than 0.1 m s^{-1}. Wind tunnel results point out significant increases of wind speed of around 1 m s^{-1}, for an inlet speed of 9 m s^{-1}, and of 0.7 and 0.8 m s^{-1}, at points 5 and 6, for an inflow wind speed of 3 m s^{-1}. The differences between points 5 and 6 are negligible, for both CFD and wind tunnel results, even if, theoretically, point 6 should be more affected by the green infrastructures, due to its location at the end of the street canyon.

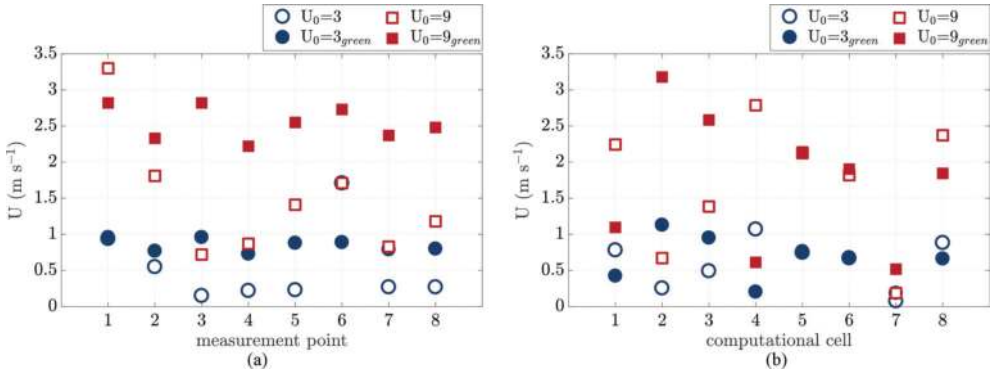

Figure 10. Comparison between the wind speed from the baseline and the green scenario: (a) measured in the wind tunnel and (b) simulated with the CFD model. These results are obtained from the numerical and physical simulations with an inflow wind blowing from West.

In conclusion, at a location nearby the implemented green areas the wind speed tends to increase, both in wind tunnel and CFD simulations. CFD and wind tunnel results do not agree at point 8, with relevant increase of wind speed predicted by the measurements, and a slight decrease of wind speed simulated by the CFD model.

4.2. Assessment of CFD performance

The CFD performance is evaluated by comparison with the wind tunnel measurements, using the validation metrics, such as the normalized mean square error (NMSE) and the fraction of simulated values within a factor of two of the measured values (FAC2), based on the metrics formula proposed by [58]. The normalized mean square error obtained for each set of wind speeds and directions ranges between 0.3 and 1 (inflow wind from Southeast and West, respectively) in the baseline scenario, while in the green scenario, the obtained NMSE ranges from 0.1 to 0.7 (inflow wind from North and Southeast, respectively). The factor FAC2 ranges between 0.9, for an inflow wind from Southeast, and 1.7, for an inflow wind from North, in the baseline scenario, and between 0.6 and 1.2 in the green scenario (over again for an inflow blowing from Southeast and North, respectively).

The acceptance criteria establish a value less than 1.5 for the NMSE. The fraction of the simulated values within a factor of two of the measured values in the wind tunnel should comprise between 0.5 and 2, following the acceptance criteria. Therefore, we can conclude that the CFD simulation results and the measured data in the wind tunnel are in good agreement, based on the acceptance criteria, for each set of wind speeds and directions, as well as for both the baseline and the green scenarios. Consequently, the obtained validation metrics confirm the ability of the CFD model to simulate the perturbation exerted by the green infrastructures on the turbulent flow dynamics.

Finally, both numerical and physical results denote the effects of green infrastructures on flow dynamics. Consequently, the demonstrated effects on flow dynamics should affect the air quality patterns.

5. Assessment of GI effects on particulate matter dispersion

Several CFD simulations were performed to assess the impact of green infrastructures on flow dynamics and, consequently, on PM10 dispersion, corresponding to **step 2** of this study. Furthermore, the comparison between the CFD simulation results and the PM10 concentrations measured at the air quality station will allow assessing the performance of the CFD model.

5.1. Assessment of CFD performance

Figure 11 presents the comparison between the hourly simulated and the measured PM10 concentrations at the AQS (in a 2 h time-basis average), on 24th September 2010. The daily averaged PM10 concentration value, from the measurements and the simulation results, is less than the established legal daily limit value of 50-μg m^{-3} (2008/50/EC Directive). **Figure 11**

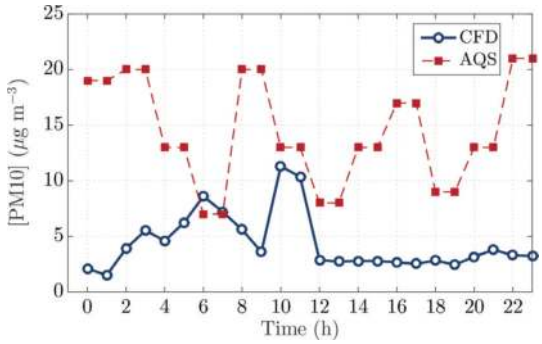

Figure 11. Comparison between hourly PM10 concentrations simulated by the CFD model and measured at the AQS.

points out a disagreement between the PM10 concentrations, simulated by the CFD model and measured at the AQS, and the traffic dynamics, mainly during night period. In addition, PM10 concentrations point out an overall underestimation by the CFD model.

The CFD performance is also evaluated using the validation metrics, i.e., the normalized mean square error and the fraction of simulated values within a factor of two of the measured values. The normalized mean square error is equal to 2.1, and the factor FAC2 is equal to 0.3. Thus, the NMSE is above the maximum value, defined equal to 1.5 as acceptance criteria, and the FAC2 is lower than the minimum accepted value of 0.5. Therefore, the CFD simulation results denote a weakness of the CFD model to simulate the impact of green infrastructures on particulate matter dispersion, when only considering the particulate matter emissions from road traffic.

5.2. Impact of GI

The impact of green infrastructures on PM10 dispersion is analyzed in an hourly basis on 24th September 2010. **Figures 12** and **13** present the differences of wind speed (**Figures 12a** and **13a**) and of PM10 concentrations (**Figures 12b** and **13b**), between the green and the baseline scenarios. These figures present the absolute differences at 1.5 m high. In addition, both **Figures 12** and **13** correspond to distinct inflow conditions in terms of emission rates; that is, **Figure 12** shows the differences at 4 am, during night and with low emission rates. **Figure 13** shows the differences at 8 am, in the morning and with high emission rates (the emission rates for each road segment are presented in **Figure 4** for these 2 h, as example).

Figure 12 shows the simulation results at 4 am initialized with a prevailing wind blowing from South-Southwest and a low wind speed of 0.3 m s^{-1}. The obtained maximum wind speed is equal to 0.79 m s^{-1}, in the baseline, and 0.84 m s^{-1}, in the green scenarios. In addition, the obtained maximum of PM10 concentration is equal to 13.6 and 29.6 μg m^{-3}, in the baseline and the green scenarios, respectively. The differences plotted in **Figure 12a** correspond to 38% of zero differences, 46% of positive differences, pointing out an overall increase of wind speed in the green scenario, and 16% of negative differences. In addition, we found 3% increases of wind speed of more than 0.1 m s^{-1} and 1% decreases of more than 0.1 m s^{-1}. **Figure 12b** denotes 69% of zero differences in PM10 concentrations, 15% of positive differences, and 16% of negative differences, indicating a similar number of occurrences of increases or decreases of PM10 concentrations. Furthermore, PM10 concentrations show 1% of increase above 0.1 μg m^{-3} and 0.5% of decrease below 0.1 μg m^{-3}.

http://dx.doi.org/10.5772/intechopen.72972

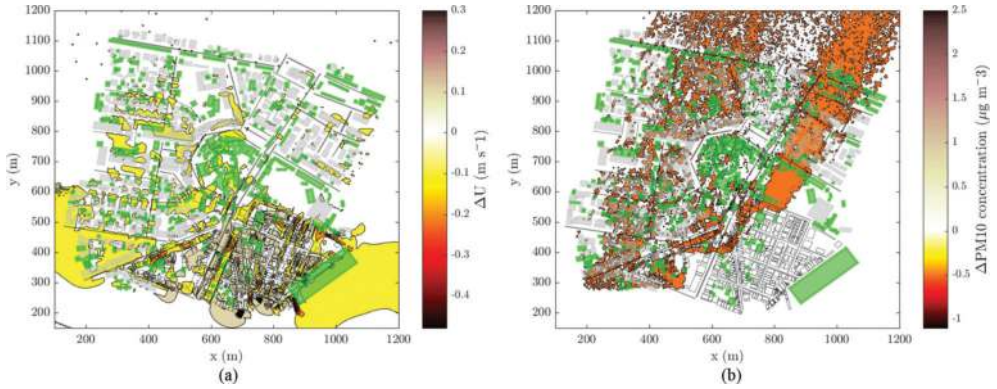

Figure 12. Horizontal iso-contour plots at 1.5 m high, at 4 am. (a) Differences of wind speed and (b) differences of PM10 concentrations between the green and the baseline scenario.

Figure 13 shows the simulation results at 8 am initialized with a prevailing wind blowing from Northwest and a wind speed of 2 m s^{-1}. The obtained maximum wind speed is equal to 4.7 m s^{-1}, in the baseline, and 4.5 m s^{-1}, in the green scenarios. In addition, the obtained maximum of PM10 concentration is equal to 16.9 and 60.3 μg m^{-3}, in the baseline and the green scenarios. The differences plotted in **Figure 13a** correspond to 39% of zero differences, 42% of positive differences, pointing out, over again, an overall increase of wind speed in the green scenario, and 19% of negative differences. Moreover, we found 4% increases of wind speed of more than 0.3 m s^{-1} and 3% decreases of more than 0.2 m s^{-1}. **Figure 13b** denotes 64% of zero differences in PM10 concentrations, 20% of positive differences and 16% of negative differences, indicating a similar number of occurrences of increases or decreases of PM10 concentrations. In addition, PM10 concentrations show 3% of increase above 0.1 μg m^{-3} and 0.8% of decrease below 0.1 μg m^{-3}.

Therefore, the implementation of green infrastructures promotes slight increases and decreases of wind speed. Specifically, the results denote a maximum increase of 0.34 m s^{-1} and a maximum decrease of 0.48 m s^{-1}, at 4 am, while at 8 am the variations of wind speed are found more

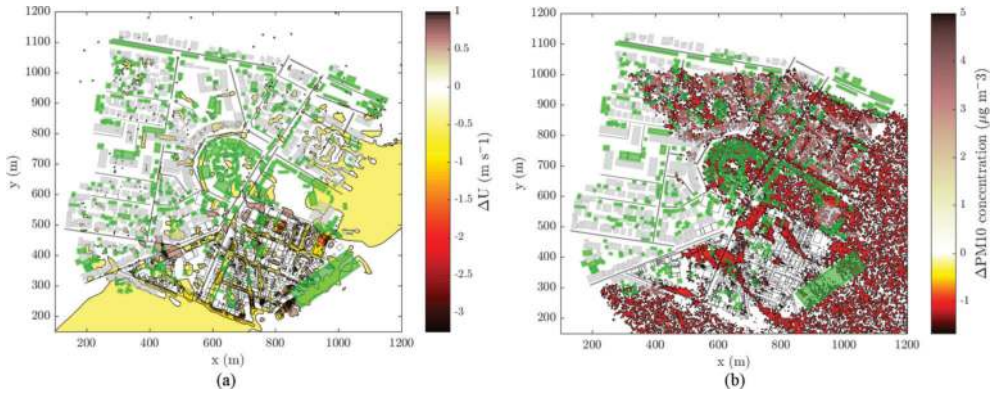

Figure 13. Horizontal iso-contour plots at 1.5 m high, at 8 am. (a) Differences of wind speed and (b) differences of PM10 concentrations between the green and the baseline scenario.

significant, with a maximum increase of 1.5 m s^{-1} and a maximum decrease of 3.3 m s^{-1}. These extreme variations of wind speed are recorded within the implemented green areas and in its surroundings. The perturbations exerted by GI on flow dynamics are more significant for higher inflow wind speeds. Consequently, these perturbations influence also the PM10 dispersion. Thus, the PM10 dispersion results in the green scenario point out an increase of PM10 concentrations of 3 μg m^{-3}, at 4 am, and of 6 μg m^{-3} at 8 am, and a maximum decrease in concentrations of 1.1 μg m^{-3}, at 4 am, and of 2 μg m^{-3}, at 8 am. The magnitude of the PM10 concentration variations is greater at 8 am, than at 4 am, mainly due to the distinct inflow conditions in terms of wind speed and emission rates.

Theoretically, increases of wind speed ($\Delta U > 0$) in a green scenario will led to enhanced dispersion of particulate matter, with lower concentrations in the green scenario ($\Delta C < 0$), compared to the baseline. On the contrary, a decrease of wind speed ($\Delta U < 0$) in a green scenario will promote the retention of pollutants, with an increase of PM10 concentrations ($\Delta C > 0$). However, for positive differences of wind speed, at 4 am, we have found 13% of positive and 10% of negative differences of PM10 concentrations (plus 19% of zero differences of concentrations), while for negative differences of wind speed, we have found 6% of positive and 5% of negative differences of PM10 concentrations (plus 8% of zero differences). Zero differences of wind speed mostly correspond to zero differences of concentrations (36%), with negligible positive and negative differences (~3%). At 8 am, positive differences of wind speed led to 7% of positive and 7% of negative differences of PM10 concentrations (plus 32% of zero differences of concentrations), while for negative differences of wind speed, we have found 2% of positive and 2% of negative differences of PM10 concentrations (plus 12% of zero differences). Zero differences of wind speed mostly correspond to zero differences of concentrations (25%), with a total of positive and negative differences equal to 14%. These results point out a nonlinear relationship between the wind speed and consequent pollutant dispersion patterns.

In conclusion, the overall effects of green infrastructures on air quality show that local air quality is strongly dependent on the linkages between meteorological conditions, the urban morphology and the emission rates.

A new set of CFD simulations were performed to assess the impact of green infrastructures on flow dynamics and, consequently, on PM10 dispersion, under recent past and medium-term future climate, corresponding to **step 3** of this study. The climate results presented in section 3.4 pointed out a decrease in the number of days with moderate to strong wind speed and an increase of low wind speed conditions, unfavorable conditions to air pollutant dispersion. Thus, CFD simulations under climate change were performed for the four cardinal directions, north, east, south and west, and the four intercardinal directions, northeast, southeast, southwest and northwest, for inflow wind speed representative of low wind speed conditions, i.e., 1 m s^{-1}, and for strong wind conditions, 6 m s^{-1}. The set of emission rates for each road segment obtained at 4 am, as example of low emission rates, and at 8 am, as example of high emission rates, was used as inflow conditions.

The effects of green infrastructures depend on inflow meteorological conditions and emission rates. Considering only the changes on the flow dynamics in medium-term climate, i.e., changes almost negligible in wind speed, the assessment of the effects of green infrastructures

procedure is similar to the one performed previously to the baseline climate (in 2010). The obtained conclusions for the baseline climate are also valid for medium-term future climate. The advantages of GI found in **Figures 12** and **13**, as well as the disadvantages, can be linearly predicted to medium-term climate.

6. Conclusions

The increased occurrence of extreme weather events and air pollution episodes, because of climate change, can cause a wide range of impacts on society, economy and environment.

This chapter presents a CFD model as a valid tool to assess climate change effects at local scale, and the role of green infrastructures as adaptation measures to increase resilience of urban areas. The CFD model presents a good performance for the simulation of flow dynamics. However, the model presents some weakness to simulate particulate matter dispersion. Therefore, the understanding of the influence of turbulent flow dynamics and the distinct emission sources contributing to fine particulate matter pollution still present a set of uncertainties. Furthermore, the most relevant conclusion of this analysis is the lack of understanding of the overall effects of GI on flow dynamics and pollutant dispersion. Future efforts should focus on the improvement of our understanding of the overall perturbations exerted by urban vegetation on the urban boundary layer.

Climate-driven changes in meteorology may also modify the natural emission patterns. In addition, future climate will also affect human activities, leading to an impact over the anthropogenic emissions. These key parameters should be taken into account, and as ongoing work on future projections of emissions, scenarios are being considered at local-scale simulations.

The results of this study present an important contribution to develop a set of adaptation measures, supported by scientific-based knowledge, from urban to district and street level, considering the geographical, demographical, economic and environmental characteristics of each urban area.

Acknowledgements

The authors would like to acknowledge the financial support of CLICURB project (EXCL/AAG-MAA/0383/2012), supported in the scope of the European Funds through COMPETE and by National Funds through the Portuguese Science Foundation (FCT) within project PEst-C/MAR/LA0017/2013. The authors further acknowledge COST Action FP1204 "Green Infrastructures Approach: linking environmental with social aspects in studying and managing urban forests" (GreenInUrbs). The authors also acknowledge the Portuguese "Ministério da Ciência, Tecnologia e Ensino Superior" for the PhD grants of Sandra Sorte (SFRH/BD/117164/2016) and Sandra Rafael (SFRH/BD/103184/2014).

Author details

Vera Rodrigues[1]*, Sandra Rafael[1], Sandra Sorte[1], Sílvia Coelho[1], Hélder Relvas[1], Bruno Vicente[1], Joana Leitão[1,2], Myriam Lopes[1], Ana Isabel Miranda[1] and Carlos Borrego[1]

*Address all correspondence to: vera.rodrigues@ua.pt

1 CESAM & Department of Environment and Planning, University of Aveiro, Aveiro, Portugal

2 Institute for Advanced Sustainability Studies (IASS), Potsdam, Germany

References

[1] EEA. The European Environment—State and Outlook 2015: Synthesis and Report. Copenhagen: European Environment Agency; 2015

[2] Ciscar JC, Feyen L, Soria A, et al. Climate Impacts in Europe. The JRC PESETA II Project. Publications Office of the European Union: European Commission, Joint Research Centre, Institute for Prospective Technological Studies; 2014

[3] Field CB, Barros VR, Mach KJ, et al. Climate Change 2014: Impacts, Adaptation, and Vulnerability. Part A: Global and Sectoral Aspects. Contribution of Working Group II to the Fifth Assessment Report of the Intergovernmental Panel on Climate Change. Cambridge, United Kingdom and New York, NY, USA: Cambridge University Press; 2014

[4] UN-HABITAT/WHO. Hidden Cities: Unmasking and Overcoming Health Inequities in Urban Settings. World Health Organization: The WHO Centre for Health Development, Kobe, and United Nations Human Settlements Programme (UN-HABITAT); 2010

[5] United Nations (UN). World Urbanization Urban Prospects: The 2014 Revision, Highlights. United Nations: Department of Economic and Social Affairs, Population Division; 2014. DOI: Report ST/ESA/SER.A/352

[6] EEA. Urban adaptation to climate change in Europe 2016: Transforming cities in a changing climate. Copenhagen: European Environment Agency; 2016. DOI: Report no 12/2016

[7] Roy S, Byrne J, Pickering C. A systematic quantitative review of urban tree benefits, costs and assessment methods across cities in different climatic zones. Urban Forestry & Urban Greening. 2012;**11**:351-363

[8] Churkina G, Grote R, Butler TM, Lawrence M. Natural selection? Picking the right trees for urban greening. Environmental Science and Policy. 2015;**47**:12-17

[9] O'Brien L, De Vreese R, Kern M, Sievänen T, Stojanova B, Atmis E. Cultural ecosystem benefits of urban and peri-urban green infrastructure across different European countries. Urban Forestry & Urban Greening. 2017;**24**:236-248

[10] Grote R, Samson R, Alonso R, Amorim JH, Cariñanos P, Churkina G, Calfapietra C. Functional traits of urban trees: Air pollution mitigation potential. Frontiers in Ecology and the Environment. 2016;**14**(10):543-550

[11] Carrus G, Scopelliti M, Lafortezza R, Colangelo G, Ferrini F, Salbitano F, Agrimi M, Portoghesi L, Semenzato P, Sanesi G. Go greener, feel better? The positive effects of biodiversity on the well-being of individuals visiting urban and peri-urban green areas. Landscape and Urban Planning. 2015;**134**:221-228

[12] Zuvela-Aloise M, Koch R, Buchholz S, Früh B. Modelling the potential of green and blue infrastructure to reduce urban heat load in the city of Vienna. Climatic Change. 2016;**135**:425-438

[13] Steeneveld GJ, Koopmans S, Heusinkveld BG, Theeuwes NE. Refreshing the role of open water surfaces on mitigating the maximum urban heat island effect. Landscape and Urban Planning. 2014;**121**:92-96

[14] Theeuwes NE, Solcerova A, Steeneveld GJ. Modelling the influence of open water surfaces on the summertime temperature and thermal comfort in the city. Journal of Geophysical Research Atmospheres. 2013;**118**(16):8881-8896

[15] Roth M. Review of atmospheric turbulence over cities. Quarterly Journal of Royal Meteorological Society. 2000;**126**:941-990

[16] Oke TR. Initial Guidance to Obtain Representative Meteorological Observations at Urban Sites. Geneva: World Meteorological Organization; 2016. Reference Report: WMO/TD no 1250

[17] Blackman K, Perret L, Savory E, Piquet T. Field and wind tunnel modelling of an idealized street canyon flow. Atmospheric Environment. 2015;**106**:139-153

[18] Masson V, Gomes L, Pigeon G, Liousse C, Pont V, Lagouarde J-P, Voogt J, Salmond J, Oke TR, Hidalgo J, Legain D, Garrouste O, Lac C, Connan O, Briottet X, Lachérade S, Tulet P. The canopy and aerosol particles interactions in TOulouse urban layer (CAPITOUL) experiment. Meteorology and Atmospheric Physics. 2008;**102**:135-157

[19] Lateb M, Meroney RN, Yataghene M, Fellouah H, Saleh F, Boufadel MC. On the use of numerical modelling for near-field pollutant dispersion in urban environments—A review. Environmental Pollution. 2016;**208**(Part A):271-283

[20] Connan O, Laguionie P, Maro D, Hébert D, Mestayer P, Rodriguez F, Rodrigues V, Rosant J-M. Vertical and horizontal concentration profile from a tracer experiment in a heterogeneous urban area. Atmospheric Research. 2015;**154**:126-137

[21] Franzese P, Huq P. Urban dispersion modelling and experiments in the daytime and nighttime atmosphere. Boundary-Layer Meteorology. 2011;**139**:395-409

[22] Carpentieri M, Hayden P, Robins AG. Wind tunnel measurements of pollutant turbulent fluxes in urban intersections. Atmospheric Environment. 2012;**46**:669-674

[23] Chavez M, Hajra B, Stathopoulos T, Bahloul A. Near-field pollutant dispersion in the built environment by CFD and wind tunnel simulations. Journal of Wind Engineering and Industrial Aerodynamics. 2011;**99**:330-339

[24] Efthimiou GC, Berbekar E, Harms F, Bartzis JG, Leitl B. Prediction of high concentrations and concentration distribution of a continuous point source release in a semi-idealized urban canopy using CFD-RANS modelling. Atmospheric Environment. 2015;**100**:48-56

[25] Di Sabatino S, Buccolieri R, Pulvirenti B, Britter R. Simulations of pollutant dispersion within idealised urban-type geometries with CFD and integral models. Atmospheric Environment. 2007;**41**:8316-8329

[26] Blocken B, Janssen WD, van Hooff T. CFD simulations for pedestrian wind comfort and wind safety in urban areas: General decision framework and case study for the Eindhoven University campus. Environmental Modelling & Software. 2012;**30**:15-34

[27] Blocken B. 50 years of computational wind engineering: Past, present and future. Journal of Wind Engineering and Industrial Aerodynamics. 2014;**129**:69-102

[28] Blocken B, Tominaga Y, Stathopoulos T. CFD simulation of micro-scale pollutant dispersion in the built environment. Building and Environment. 2013;**64**:225-230

[29] Tominaga Y, Stathopoulos T. CFD simulation of near-field pollutant dispersion in the urban environment: A review of current modeling techniques. Atmospheric Environment. 2013;**79**:716-730

[30] Hofman J, Bartholomeus H, Janssem S, Calders K, Wuyts K, van Wittenberghe S, Samson R. Influence of tree crown characteristics on the local PM10 distribution inside an urban street canyon in Antwerp (Belgium): A model and experimental approach. Urban Forestry & Urban Greening. 2016;**20**:265-276

[31] Amorim JH, Rodrigues V, Tavares R, Valente J, Borrego C. CFD modelling of the aerodynamic effect of trees on urban air pollution dispersion. Science of the Total Environment. 2013;**461**-**462**:541-551

[32] Abhijth KV, Kumar P, Gallagher J, McNabola A, Baldauf R, Pilla F, Broderick B, Di Sabatino S, Pulvirenti B. Air pollution abatement performances of green infrastructures in open road and built-up street canyon environments—A review. Atmospheric Environment. 2017;**162**:71-86

[33] Vos P, Maiheu B, Vankerkom J, Janssen S. Improving local air quality in cities: To tree or not to tree? Environmental Pollution. 2013;**183**:113-122

[34] Gromke C, Blocken B. Influence of avenue-trees on air quality at th urban neighborhood scale: Part II: Traffic pollutant concentrations at pedestrian level. Environmental Pollution. 2015;**196**:176-184

[35] Buccolieri R, Salim S, Leo L, Di Sabatino S, Chan A, Ielpo P, de Gennaro G, Gromke C Analysis of local scale tree-atmosphere interaction on pollutant concentration in idealized street canyons and application to a real urban junction. Atmospheric Environment. 2011;**45**:1702-1713

[36] Jeanjean APR, Monks PS, Leigh RJ. Modelling the effectiveness of urban trees and grass on PM2.5 reduction via dispersion and deposition at city scale. Atmospheric Environment. 2016;**147**:1-10. DOI: 10.1016/j.atmosenv.2016.09.033

[37] Salmond JA, Williams DE, Laing G, Kingham S, Dirks K, Longley I, Henshaw GS. The influence of vegetattion on the horizontal and vertical distribution of pollutants in a street canyon. Science of the Total Environment. 2013;**443**:287-298

[38] Janhäll S. Review on urban vegetation and particle air pollution—Deposition and dispersion. Atmospheric Environment. 2015;**105**:130-137. DOI: 10.1016/j.atmosenv.2015.01.052

[39] Sá E, Martins H, Ferreira J, Marta-Almeida M, Rocha A, Carvalho A, Freitas S, Borrego C. Climate change and pollutant emissions impacts on air quality in 2050 over Portugal. Atmospheric Environment. 2016;**131**:209-224

[40] Markakis K, Valari M, Colette A, Sanchez O, Perrussel O, Honore C, Vautard R, Klimont Z, Rao S. Air quality in the mid-21st century for the city of Paris under two climate scenarios; from the regional to local scale. Atmospheric Chemistry and Physics. 2014;**14**:7323-7340

[41] Skamarock WC, Klemp JB, Dudhia J, Gill DO, Barker DM, Huang XY, Wang W, Powers JG. A description of the Advanced Research WRF version 3. NCAR/TN-475+STR. Boulder, Colorado, USA: National Center for Atmospheric Research; 2008. 113 pp

[42] IPCC. Climate Change 2013: The Physical Basis. In: Stocker TF, Qin D, Plattner G-K, Tignor M, Allen SK, Boschung J, Nauels A, Xia Y, Bex V, Midgley PM, editors. Contribution of Working Group I to the Fifth Assessment Report of the Intergovernmental Panel on Climate Change. Cambridge, United Kingdom and New York, NY, USA: Cambridge University Press; 2013. 1535 pp

[43] Giorgetta MA, Jungclaus J, Reick CH, Legutke S, Bader J, Böttinger M, et al. Climate and carbon cycle changes from 1850 to 2100 in MPI-ESM simulations for the coupled model Intercomparison project phase 5. Journal of Advances in Modeling Earth Systems. 2013;**5**(3):572-597

[44] Launder BE, Spalding DB. The numerical computation of turbulent flows. Computer Methods in Applied Mechanics and Engineering. 1974;**3**(2):269-289

[45] Green S. Modelling turbulent air flow in a stand of widely spaced trees. Journal of Computational Dynamics and its Applications. 1992;**5**(3):294-312

[46] Katul GG, Mahrt L, Poggi D, Sanz C. One- and two-equation models for canopy turbulence. Boundary-Layer Meteorology. 2004;**113**(1):81-109

[47] Kaimal JC, Finnigan JJ. Atmospheric Boundary Layer Flows: Their Structure and Measurement. New York: Oxford University Press; 1994. p. 4289

[48] Poggi D, Porporato A, Ridolfi L, Albertson JD, Katul GG. The effect of vegetation density on canopy sub-layer turbulence. Boundary-Layer Meteorology. 2004;**111**(3):565-587

[49] Raupach MR, Shaw RH. Averaging procedures for flow within vegetation canopies. Boundary-Layer Meteorology. 1982;**22**(1):79-90

[50] Borrego C, Tchepel O, Costa AM, Amorim JH, Miranda AI. Emission and dispersion modelling of Lisbon air quality at local scale. Atmospheric Environment. 2003;**37**:5197-5205

[51] Dimitrova R, Sini J-F, Richards K, Schatzmann M, Weeks M, Perez Garcia E, Borrego C. Influence of thermal effects on the wind field within the urban environment. Boundary-Layer Meteorology. 2009;**131**(2):223-243

[52] Vardoulakis S, Dimitrova R, Richards K, Hamlyn D, Camilleri G, Weeks M, Sini J-F, Britter R, Borrego C, Schatzmann M, Moussiopoulos N. Numerical model inter-comparison for

wind flow and turbulence around single-block buildings. Environment Modeling & Assessment. 2011;**16**:169-181

[53] INE. Censos 2011. Resultados Definitivos—Região Norte: XV recenseamento geral da população e V recenseamento geral da habitação. Lisboa: Instituto Nacional de Estatística. p. 2013

[54] Instituto Português do Mar e da Atmosfera (IPMA). IPMA [Internet]. Available from: https://www.ipma.pt/pt/educativa/tempo.clima/ [Accessed: 07 July 2017]

[55] EEA. EMEP/EEA air pollutant emission inventory guidebook 2009. Technical guidance to prepare national emission inventories. Technical report no 9/2009. Copenhagen, Denmark

[56] CENSUS, 2011. Statistical Data for Portugal [Internet]. 2011. Available from: http://censos.ine.pt

[57] ANSSFP. Autoridade Nacional de Supervisão de Seguros e Fundos de Pensões [Internet]. 2011. Available from: http://www.asf.com.pt

[58] Chang J, Hanna S. Air quality model performance evaluation. Meteorology and Atmospheric Physics. 2004;**87**:167-196